The Astrophysical Journal, 522:983–990, 1999 September 10

BLUE STRAGGLER STARS: THE SPECTACULAR POPULATION IN M80[1]

Francesco R. Ferraro,[2,3] Barbara Paltrinieri,[4] Robert T. Rood,[5] and Ben Dorman[6]
Received 1999 March 19; accepted 1999 April 10

ABSTRACT

Using *Hubble Space Telescope* WFPC2 observations in two ultraviolet (UV) filters (F225W and F336W) of the central region of the high-density Galactic globular cluster (GGC) M80, we have identified 305 blue straggler stars (BSS), which represents the largest and most concentrated population of BSS ever observed in a GGC. We also identify the largest clean sample of evolved BSS yet found. The high stellar density alone cannot explain the BSS, and we suggest that in M80 we are witnessing a transient dynamical state, during which stellar interactions are delaying the core-collapse process leading to an exceptionally large population of *collisional* BSS.

Subject headings: blue stragglers — globular clusters: individual (M80) — stars: evolution — ultraviolet: stars

1. INTRODUCTION

Blue straggler stars (BSS) were first observed in the 1950s (Sandage 1953) in the Galactic globular cluster (GGC) M3. In the color-magnitude diagram they formed a sparsely populated sequence extending to higher luminosities than the turnoff point of normal hydrogen-burning main-sequence stars. Superficially they looked like a population of younger stars, more massive than the turnoff stars, in an old star cluster. Since there is no other indication of star formation after the burst that formed the bulk of the cluster stars, two mechanisms for making BSS are favored. First is the merger of two stars in a primordial binary system, where "primordial" refers to binaries formed when the cluster formed. Second are collisions in regions of very high stellar density (Hills & Day 1976; Fusi Pecci et al. 1992; Ferraro et al. 1993; Ferraro, Fusi Pecci, & Bellazzini 1995; Bailyn 1995; Meylan & Heggie 1997). These collisional BSS include several classes of objects: direct collisions producing a more massive star; collisions that harden primordial binaries until the point of merger; and binaries produced in collisions that later merge. The dense cores of globular clusters were obvious targets for observations required to refine our understanding of BSS. Indeed, more than 20 yr ago Hills & Day (1976) suggested searching the core of M80 for collisional BSS. However, only with the advent of the *Hubble Space Telescope* (*HST*) could such observations be made (Paresce et al. 1991; Ferraro & Paresce 1993; Ferraro et al. 1997a; Drissen & Shara 1998; Guhathakurta et al. 1998).

The BSS population, especially collisional BSS, can serve as a diagnostic for the dynamical evolution of GGCs. Because of gravitational interactions between cluster stars, GGCs evolve dynamically on timescales generally smaller than their ages. For example, the first manifestation of a dynamical process within a GGC is that in the inner part of a GGC more massive stars (or binaries) should settle toward the center. Beyond this, more dramatic dynamical phases can happen during the cluster's lifetime. Stars with velocities above the escape velocity continuously evaporate, and phenomena such as Galactic tidal stripping remove stars from the outer regions of the cluster and induce substantial changes in the structure of the cluster itself. As a GGC adjusts to the loss of stars, the cluster core must contract. Under some circumstances this process can run away, leading to a possibly catastrophic "core collapse." About 15% of the GGC population show evidence for this phenomenon. Binaries are thought to play a fundamental role in the core collapse: binary-binary collisions could in fact be effective in halting (or, more probably, delaying) the collapse of the core, avoiding infinite central density.

This time of enhanced binary interactions as the cluster fights off core collapse could well correspond to a period of unusually large BSS production. By the end of this phase most of the binaries in the core will be destroyed by close encounters; the survivors will become highly hardened (i.e., tightly bound), producing most of the additional collisional BSS.

2. OBSERVATIONS

To search for BSS (and other blue objects), we have used the Wide Field Planetary Camera (WFPC2) onboard *HST* to obtain UV and visible images of the central region of the high-density cluster M80 (NGC 6093). Both the high angular resolution and UV sensitivity of *HST* are essential to identify these UV-bright objects among the much more luminous red giants in the cluster (Ferraro et al. 1997a). The images were obtained on 1996 April 5–6 (GO-5903, PI: F. R. Ferraro) with the WFPC2 F160BW (far-UV), F255W (mid-UV), F336W (*U*), and F555W (visible or *V*) filters. The planetary camera (PC, which has the highest resolution $\sim 0\farcs046$ pixel^{-1}) was roughly centered on the cluster center, while the wide field (WF) cameras (at lower resolution $\sim 0\farcs1$ pixel^{-1}) sampled the surrounding outer regions. The BSS identifications are based on 4×600 s exposures in *U* and 4×300 s exposures in F255W. The WFPC2 frames were processed through the standard *HST* WFPC pipeline, and photometry was

[1] Based on observations with the NASA/ESA *Hubble Space Telescope*, obtained at the Space Telescope Science Institute, which is operated by AURA, Inc., under NASA contract NAS5-26555.

[2] European Southern Observatory, Karl Schwarzschild Strasse 2, D-85748 Garching bei München, Germany.

[3] Osservatorio Astronomico di Bologna, Via Ranzani 1, 40127 Bologna, Italy.

[4] Instituto di Astronomia-Università "La Sapienza," Piazzale Aldo Moro 5, 00185 Roma, Italy.

[5] Astronomy Department, University of Virginia, P.O. Box 3818, Charlottesville, VA 22903-0818.

[6] Raytheon STX and Laboratory for Astronomy and Solar Physics, Code 681, NASA/GSFC, Greenbelt, MD 20771.

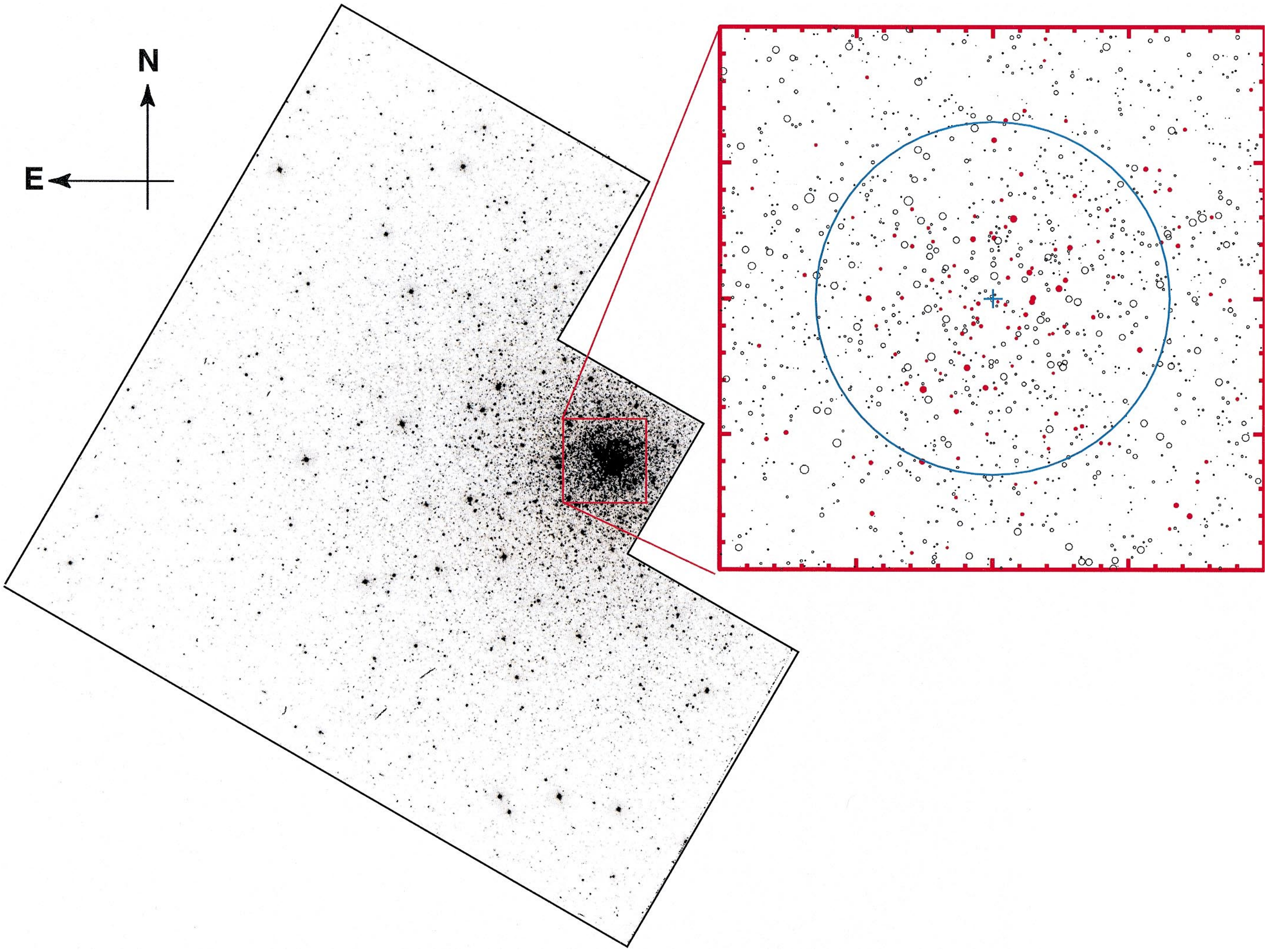

FIG. 1.—*V*-band WFPC2 image (*background*) of M80 (*negative grayscale*) and (*foreground*) a zoomed map (in the UV F255W filter) of the cluster's central 10″ × 10″ region. The red stars indicate the identified blue stragglers. The blue circle has a radius of 6″.5 from the cluster center of gravity (which is indicated by a heavy blue +). It corresponds to the core radius of the cluster (r_c) as determined by this study. The brightest objects in the zoomed image are HB stars. Both the HB and BSS are easily identified in contrast to the *V* image, which is dominated by the red giants.

obtained as outlined in our study of BSS in M3 (Ferraro et al. 1997a). Figure 1 shows the advantages of using UV images to search for BSS: in the center of the *V* image the light from the bright red giant branch (RGB) stars blends together. In the UV image the brightest objects are horizontal branch (HB) stars and BSS; there is little blending even at the center.

3. RESULTS

The UV color-magnitude diagram (CMD) in the (m_{255}, $m_{255} - U$) plane for more than 13,000 stars identified in the *HST* field of view is presented in Figure 2. The large population of BSS defines a narrow, nearly vertical sequence spanning $\sim$3 mag in m_{255}. They are clearly separable from the cooler and fainter turnoff and subgiant branch (SGB) stars. However, as already discussed in previous papers (see Ferraro et al. 1995), one of the major problems in defining homogeneous samples of BSS is the *operative* definition of the faint edge of the BSS population. This is true even in UV CMDs (see, for example, Ferraro et al. 1997a), since generally the BSS sequence merges smoothly into the main-sequence turnoff region without showing any gap or discontinuity. In selecting the BSS

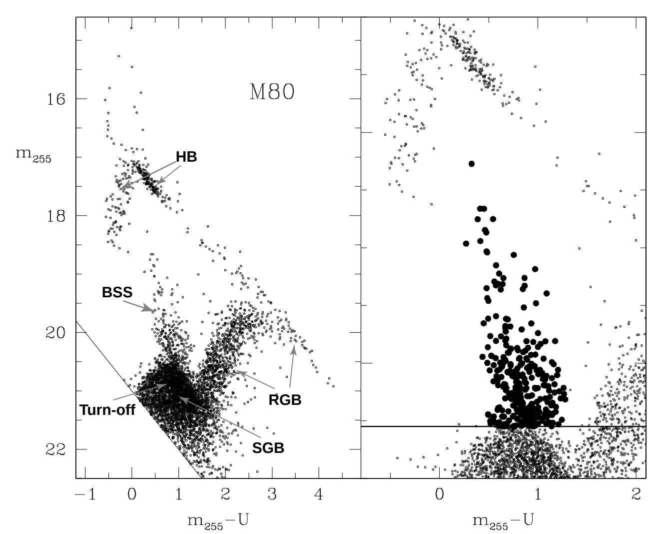

FIG. 2.—(m_{255}, $m_{255} - U$) CMD for the central region of M80. *Left-hand panel*: The whole CMD. The solid line corresponds to $U = 21$. *Right-hand panel*: The zoomed CMD in the BSS region. BSS are plotted as filled circles. The heavy horizontal line at $m_{255} = 20.55$ corresponds to the assumed limiting magnitude for the selected BSS.

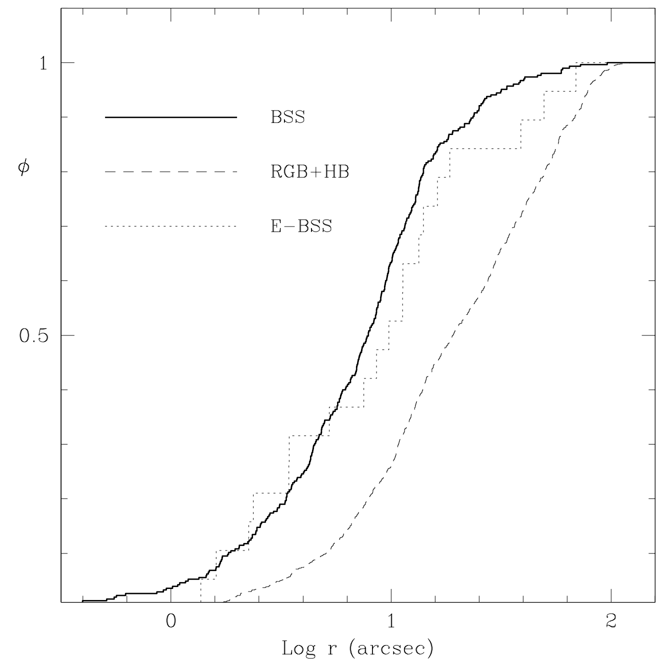

FIG. 3.—Cumulative radial distribution (ϕ) for BSS (*heavy solid line*) and E-BSS (*dotted line*) compared to the HB+RGB stars (*dashed line*) as a function of their projected distance (r) from the cluster center.

sample, we have adopted the same criteria we used in M3, which was recently observed (Ferraro et al. 1997a) with the same technique and setup used here. In order to assure the same BSS limiting absolute magnitude for M80 as we adopted in M3, we aligned the two (m_{255}, $m_{255} - U$) CMDs, using the bright portion of the HB as the *normalization* region. The shift in magnitude required to align the two CMDs is $\delta m_{255} = 1.15$. The resulting fainter boundary of the BSS sequence in M80 is $m_{255} = 20.55$. Adopting this figure, M80 turns to have a spectacularly large population of BSS: 305 candidates have been found in the WFPC2 field of view.

Ferraro et al. (1997a) split the M3 BSS into *bright* and *faint* subsamples. The analogous division in M80 is at $m_{255} = 20.15$. M80 has (1) 129 bright BSS with $m_{255} < 20.15$, and (2) 176 faint BSS with $20.15 < m_{255} < 20.55$.

The BSS region in the CMD is better shown in Figure 2 (*left-hand panel*) where the total sample of BSS is plotted as filled circles. Note that the limiting magnitude for the faint BSS is at the "error envelope" of the main-sequence region on the CMD. By examining the adjacent regions of the CMD, we estimate that there are at most a few MS stars misidentified as BSS. In addition, the faint BSS and bright BSS have almost identical radial distributions, while that of the MS stars is much less centrally concentrated, similar to that of the RGB+HB stars (see Fig. 3). This again suggests at most a very minor contamination of the faint BSS sample.

Table 1 lists the BSS candidates: the column (1) is the number, and in columns (2)–(5) we report the identification number, m_{255} and U magnitudes, and the coordinates (X, Y), respectively. The coordinates are referred to an arbitrary system and are expressed in *ground-based* pixel units (1 pixel = 0".35) after a rotation and translation to match the complementary ground-based observations (see below).

While not obvious from Figure 1, Figure 3 clearly shows that the BSS (*heavy solid line*) are far more concentrated

TABLE 1

THE BSS POPULATION IN M80

Name	Identification	m_{255}	U	X	Y
BSS 1	13166	18.272	17.946	673.806	609.805
BSS 2	13676	18.661	18.248	678.657	655.898
BSS 3	43933	18.662	18.210	650.530	605.157
BSS 4	10338	18.751	18.207	614.898	649.000
BSS 5	14551	18.753	18.365	669.207	637.937
BSS 6	14973	18.846	18.384	683.438	648.577
BSS 7	43603	18.867	18.392	652.347	601.041
BSS 8	20052	18.942	18.527	614.882	667.532
BSS 9	11193	18.964	18.694	673.794	640.225
BSS 10......	13786	19.032	18.554	709.550	645.030
BSS 11......	14804	19.040	18.556	669.121	630.334
BSS 12......	13180	19.062	18.307	673.960	612.312
BSS 13......	15327	19.152	18.577	680.614	647.182
BSS 14......	11215	19.185	18.213	663.463	647.503
BSS 15......	15329	19.224	18.618	680.730	647.575
BSS 16......	15356	19.262	18.398	680.337	650.271
BSS 17......	14208	19.263	18.614	675.750	638.118
BSS 18......	13834	19.293	18.736	706.016	652.431
BSS 19......	11184	19.313	18.719	697.225	624.590
BSS 20......	11610	19.315	18.674	674.402	653.767
BSS 21......	10850	19.326	18.753	630.984	656.546
BSS 22......	14639	19.330	18.465	684.581	652.878
BSS 23......	21847	19.350	18.872	518.844	709.890
BSS 24......	43935	19.358	18.511	650.218	603.417
BSS 25......	11978	19.362	18.740	676.616	664.153
BSS 26......	11605	19.396	18.307	691.932	642.124
BSS 27......	11663	19.436	18.951	684.123	649.454
BSS 28......	14562	19.460	18.963	695.810	625.733
BSS 29......	13387	19.481	18.500	672.694	635.620
BSS 30......	12229	19.518	18.661	692.561	661.135
BSS 31......	15257	19.593	19.019	676.614	653.890
BSS 32......	43749	19.615	19.121	695.164	578.106
BSS 33......	10628	19.616	18.940	654.840	633.363
BSS 34......	14496	19.621	18.927	663.863	624.841
BSS 35......	10357	19.655	19.206	665.331	616.820
BSS 36......	15212	19.656	18.723	674.464	644.874
BSS 37......	15344	19.678	19.008	679.951	645.845
BSS 38......	12032	19.683	18.963	695.952	653.085
BSS 39......	10703	19.697	19.028	663.739	630.209
BSS 40......	12408	19.708	18.873	659.253	688.351
BSS 41......	14383	19.726	19.053	677.829	666.232
BSS 42......	12212	19.740	18.739	695.089	658.973
BSS 43......	13221	19.766	19.250	652.808	632.693
BSS 44......	13547	19.768	19.143	670.100	649.470
BSS 45......	11923	19.788	19.109	679.463	660.599
BSS 46......	13813	19.806	19.137	660.437	679.883
BSS 47......	13497	19.808	19.234	685.882	634.075
BSS 48......	14261	19.809	18.634	674.965	647.004
BSS 49......	15206	19.810	18.926	673.290	643.834
BSS 50......	14365	19.811	18.735	685.082	658.333
BSS 51......	13238	19.817	18.864	689.182	610.791
BSS 52......	14584	19.834	18.807	668.031	653.008
BSS 53......	11160	19.845	19.167	656.767	649.971
BSS 54......	15180	19.860	18.859	694.186	653.441
BSS 55......	13380	19.862	19.371	667.483	638.571
BSS 56......	15111	19.867	18.967	687.050	645.576
BSS 57......	12270	19.869	19.079	708.024	652.182
BSS 58......	11316	19.874	19.153	698.037	628.225
BSS 59......	15217	19.876	19.148	675.268	644.626
BSS 60......	20127	19.888	19.091	639.743	709.130
BSS 61......	13487	19.892	19.019	683.171	635.413
BSS 62......	10845	19.904	19.054	652.011	642.520
BSS 63......	15094	19.909	19.214	679.814	667.246
BSS 64......	15365	19.911	19.207	678.079	649.712
BSS 65......	11461	19.926	18.952	666.185	654.131
BSS 66......	12847	19.929	18.999	706.911	673.669
BSS 67......	13302	19.936	19.411	679.628	624.777
BSS 68......	12060	19.939	19.409	643.727	687.863
BSS 69......	14825	19.946	19.509	685.224	633.806

TABLE 1—*Continued*

Name	Identification	m_{255}	U	X	Y
BSS 70	13494	19.948	19.297	647.515	659.453
BSS 71	31752	19.955	19.140	563.856	625.901
BSS 72	13541	19.957	19.386	698.976	630.335
BSS 73	13908	19.958	19.074	696.672	665.286
BSS 74	13503	19.961	18.903	666.971	647.575
BSS 75	43763	19.963	19.155	657.903	511.669
BSS 76	15006	19.971	19.305	688.498	656.824
BSS 77	30428	19.971	19.080	507.443	657.791
BSS 78	15044	19.979	19.327	712.280	656.451
BSS 79	41134	19.981	19.311	636.288	589.634
BSS 80	21457	19.992	18.849	627.268	811.920
BSS 81	11652	19.996	19.379	702.232	636.957
BSS 82	13322	19.998	19.512	697.476	614.573
BSS 83	11941	19.998	19.349	699.408	647.989
BSS 84	21118	20.002	19.162	578.326	697.644
BSS 85	15101	20.006	19.071	677.816	646.873
BSS 86	14958	20.009	19.287	684.011	644.586
BSS 87	41803	20.010	18.849	668.254	580.809
BSS 88	12686	20.017	19.194	703.630	669.480
BSS 89	11241	20.018	19.467	687.897	632.313
BSS 90	10881	20.019	19.386	672.884	630.670
BSS 91	15216	20.022	19.299	674.868	645.430
BSS 92	15335	20.026	19.059	679.280	644.419
BSS 93	15123	20.030	19.394	699.489	656.087
BSS 94	10879	20.031	19.123	647.484	647.048
BSS 95	30577	20.039	19.115	491.789	652.232
BSS 96	43669	20.042	19.153	668.734	589.252
BSS 97	15343	20.046	19.254	678.100	644.472
BSS 98	13763	20.054	19.442	646.040	684.170
BSS 99	14601	20.058	18.853	668.011	656.901
BSS 100......	43824	20.059	19.038	729.577	526.286
BSS 101......	14216	20.062	19.075	676.782	638.048
BSS 102......	10376	20.063	19.553	634.087	637.975
BSS 103......	14337	20.065	19.478	677.405	657.863
BSS 104......	14402	20.068	19.354	684.148	666.191
BSS 105......	13416	20.071	19.303	682.384	631.701
BSS 106......	14321	20.074	19.359	677.821	655.064
BSS 107......	13755	20.076	19.162	701.435	647.361
BSS 108......	14509	20.077	19.387	672.673	626.527
BSS 109......	14192	20.081	19.385	666.286	641.646
BSS 110......	14312	20.083	19.041	674.578	656.175
BSS 111......	11913	20.086	19.299	663.298	670.750
BSS 112......	13430	20.087	19.363	664.277	644.634
BSS 113......	10507	20.093	19.053	668.047	620.675
BSS 114......	14332	20.096	19.092	683.058	652.677
BSS 115......	40252	20.099	19.255	601.244	616.704
BSS 116......	15166	20.104	18.908	669.725	654.929
BSS 117......	43878	20.110	19.371	648.907	579.637
BSS 118......	43042	20.110	19.024	625.900	377.749
BSS 119......	13904	20.110	19.287	682.004	674.804
BSS 120......	14882	20.114	19.535	689.140	649.773
BSS 121......	14201	20.116	19.364	681.917	632.980
BSS 122......	15014	20.120	19.491	693.555	658.775
BSS 123......	20203	20.127	19.190	624.702	691.713
BSS 124......	15032	20.130	18.987	670.213	653.507
BSS 125......	20115	20.135	19.272	627.499	690.667
BSS 126......	15360	20.138	19.088	680.604	650.731
BSS 127......	43938	20.139	19.358	648.548	597.091
BSS 128......	15248	20.142	19.068	672.450	650.975
BSS 129......	11860	20.148	19.556	687.557	653.547
		Faint BSS			
BSS 130......	10389	20.158	19.610	642.587	632.806
BSS 131......	13396	20.159	19.373	672.170	637.232
BSS 132......	14547	20.164	19.385	675.904	633.236
BSS 133......	31788	20.166	19.299	573.854	644.047
BSS 134......	20040	20.172	19.294	674.662	756.305
BSS 135......	14237	20.174	19.365	664.719	650.635
BSS 136......	10685	20.182	19.526	661.909	630.766
BSS 137......	15244	20.183	19.014	671.914	649.863

TABLE 1—*Continued*

Name	Identification	m_{255}	U	X	Y
BSS 138......	12870	20.185	19.517	714.991	669.596
BSS 139......	13419	20.192	19.597	695.128	623.244
BSS 140......	14286	20.192	19.133	682.808	643.842
BSS 141......	11582	20.194	19.117	657.931	663.622
BSS 142......	14828	20.199	19.385	672.974	641.798
BSS 143......	15219	20.200	19.093	674.284	646.426
BSS 144......	10271	20.205	19.557	663.338	614.546
BSS 145......	12251	20.209	19.437	693.983	661.022
BSS 146......	15269	20.214	19.434	682.861	639.683
BSS 147......	12561	20.215	19.245	716.134	656.440
BSS 148......	11260	20.215	18.953	688.767	632.229
BSS 149......	15261	20.216	19.334	676.303	654.429
BSS 150......	10364	20.216	19.536	643.146	631.635
BSS 151......	14033	20.216	19.217	691.964	684.797
BSS 152......	13521	20.219	19.338	651.292	659.059
BSS 153......	15332	20.221	19.245	678.972	643.338
BSS 154......	12812	20.223	19.399	690.496	683.165
BSS 155......	12615	20.231	19.360	705.921	665.231
BSS 156......	15159	20.235	19.561	671.020	646.408
BSS 157......	14266	20.237	19.465	661.788	656.032
BSS 158......	15186	20.238	19.124	696.072	655.066
BSS 159......	13357	20.243	19.458	681.030	628.110
BSS 160......	15150	20.245	19.028	675.549	641.440
BSS 161......	15218	20.255	19.086	673.558	646.634
BSS 162......	15239	20.261	19.528	671.995	648.257
BSS 163......	14532	20.262	19.558	678.935	627.946
BSS 164......	40791	20.266	19.446	621.682	596.032
BSS 165......	14798	20.268	19.002	716.549	649.574
BSS 166......	13310	20.269	19.516	693.353	616.340
BSS 167......	13297	20.279	19.339	645.724	646.381
BSS 168......	11301	20.284	19.477	678.524	640.427
BSS 169......	10814	20.287	19.568	658.343	637.362
BSS 170......	40934	20.287	19.395	631.342	599.438
BSS 171......	40272	20.287	19.371	606.178	622.875
BSS 172......	20628	20.294	19.172	599.222	685.074
BSS 173......	15196	20.297	19.470	669.547	640.959
BSS 174......	15132	20.299	19.572	661.906	643.559
BSS 175......	14247	20.302	19.498	694.785	632.791
BSS 176......	15179	20.306	19.639	693.309	653.493
BSS 177......	22510	20.306	19.074	601.699	668.373
BSS 178......	15098	20.307	19.232	677.015	647.189
BSS 179......	30372	20.310	19.582	562.428	628.251
BSS 180......	14617	20.311	19.286	678.432	651.663
BSS 181......	14572	20.314	19.561	662.892	649.512
BSS 182......	13506	20.315	19.037	674.174	643.346
BSS 183......	14162	20.330	19.509	671.462	631.488
BSS 184......	13885	20.336	19.345	681.901	672.537
BSS 185......	11964	20.338	19.497	710.443	641.391
BSS 186......	10588	20.338	19.241	671.764	621.222
BSS 187......	14285	20.344	19.196	682.435	643.755
BSS 188......	15185	20.346	19.546	695.404	655.128
BSS 189......	14252	20.348	19.504	663.878	653.352
BSS 190......	13050	20.350	19.575	666.803	708.402
BSS 191......	20190	20.352	19.504	634.013	704.955
BSS 192......	14350	20.353	19.414	677.232	660.442
BSS 193......	14150	20.355	19.417	656.920	639.568
BSS 194......	15195	20.367	19.231	671.005	639.621
BSS 195......	12934	20.368	19.620	728.742	663.058
BSS 196......	15334	20.373	19.449	679.617	643.729
BSS 197......	12463	20.374	19.544	713.418	654.890
BSS 198......	20317	20.379	19.196	602.803	666.827
BSS 199......	13841	20.384	19.774	687.317	665.039
BSS 200......	12845	20.385	19.382	699.523	678.315
BSS 201......	14933	20.385	19.474	695.746	680.347
BSS 202......	14284	20.387	19.453	682.021	644.108
BSS 203......	14236	20.389	19.468	664.509	650.331
BSS 204......	11488	20.390	19.439	688.841	640.450
BSS 205......	14984	20.390	19.794	682.100	651.627
BSS 206......	14267	20.395	19.456	661.925	656.421
BSS 207......	20351	20.395	19.523	644.823	731.688

TABLE 1—*Continued*

Name	Identification	m_{255}	U	X	Y
BSS 208......	14114	20.402	19.321	661.224	629.283
BSS 209......	11910	20.402	19.616	703.331	644.554
BSS 210......	13690	20.403	19.590	699.971	643.245
BSS 211......	13882	20.403	19.451	689.814	667.414
BSS 212......	15100	20.405	19.816	676.426	647.330
BSS 213......	22431	20.406	19.527	642.283	737.231
BSS 214......	14127	20.410	19.772	655.388	635.092
BSS 215......	12310	20.410	19.408	702.222	657.056
BSS 216......	14531	20.413	19.558	678.742	627.527
BSS 217......	14963	20.418	19.560	685.408	643.859
BSS 218......	12422	20.418	19.718	712.591	654.067
BSS 219......	15108	20.422	19.240	686.117	645.326
BSS 220......	15153	20.423	19.630	671.364	644.742
BSS 221......	14652	20.425	19.322	665.202	667.023
BSS 222......	14270	20.426	19.410	703.610	628.765
BSS 223......	12352	20.428	19.535	681.541	671.892
BSS 224......	12857	20.429	19.494	708.919	672.940
BSS 225......	11408	20.430	19.575	648.791	663.522
BSS 226......	13309	20.433	19.354	693.686	616.011
BSS 227......	11052	20.433	19.487	667.882	639.291
BSS 228......	12266	20.437	19.282	678.006	671.974
BSS 229......	12940	20.438	19.528	728.299	663.606
BSS 230......	13584	20.438	19.579	652.013	665.324
BSS 231......	12443	20.439	19.614	666.583	684.730
BSS 232......	14881	20.445	19.952	688.595	649.890
BSS 233......	12444	20.445	19.331	672.576	680.794
BSS 234......	15104	20.449	19.951	676.364	647.734
BSS 235......	14896	20.450	19.622	688.967	654.023
BSS 236......	14362	20.450	19.307	701.938	645.824
BSS 237......	11556	20.453	19.384	662.948	659.486
BSS 238......	14605	20.454	19.547	671.446	654.854
BSS 239......	14320	20.457	19.387	678.262	654.542
BSS 240......	13569	20.458	19.483	686.270	641.558
BSS 241......	13325	20.458	19.706	661.517	637.933
BSS 242......	15214	20.459	19.562	674.919	645.062
BSS 243......	20828	20.461	19.456	586.091	679.750
BSS 244......	14972	20.463	19.718	682.140	649.020
BSS 245......	15004	20.463	19.911	690.168	655.668
BSS 246......	13797	20.464	19.827	697.571	653.898
BSS 247......	14382	20.464	19.809	677.688	665.821
BSS 248......	13336	20.466	19.608	689.062	621.485
BSS 249......	13654	20.471	19.381	689.822	647.018
BSS 250......	13229	20.474	19.487	676.311	617.896
BSS 251......	14401	20.480	19.525	686.165	664.941
BSS 252......	20733	20.482	19.525	612.826	711.935
BSS 253......	30220	20.483	19.695	476.277	701.749
BSS 254......	10565	20.483	19.442	659.843	627.875
BSS 255......	14884	20.489	19.943	690.085	649.827
BSS 256......	11911	20.491	19.248	708.752	641.008
BSS 257......	15102	20.491	19.566	678.047	647.186
BSS 258......	10931	20.494	19.547	649.233	647.593
BSS 259......	14599	20.496	19.602	676.628	651.761
BSS 260......	14942	20.498	19.792	672.602	637.606
BSS 261......	12419	20.498	19.975	699.785	662.194
BSS 262......	14552	20.501	19.459	669.193	638.541
BSS 263......	13015	20.503	19.988	693.784	689.630
BSS 264......	14748	20.506	19.680	674.291	651.745
BSS 265......	12217	20.507	19.623	702.089	654.429
BSS 266......	14993	20.510	19.616	686.722	656.283
BSS 267......	11223	20.513	19.905	693.393	628.203
BSS 268......	11552	20.513	19.971	700.215	635.018
BSS 269......	11943	20.516	19.672	676.643	663.071
BSS 270......	10806	20.517	19.400	649.510	642.744
BSS 271......	10260	20.517	19.949	669.445	610.096
BSS 272......	14276	20.517	19.396	675.725	648.328
BSS 273......	13664	20.518	19.921	688.554	649.185
BSS 274......	12380	20.518	19.366	706.500	656.701
BSS 275......	13413	20.521	19.664	674.422	636.487
BSS 276......	11715	20.524	19.434	692.627	645.562
BSS 277......	13930	20.524	20.006	715.254	654.985
BSS 278......	13420	20.525	19.524	695.694	623.308

TABLE 1—*Continued*

Name	Identification	m_{255}	U	X	Y
BSS 279......	10991	20.525	19.838	632.049	660.775
BSS 280......	13289	20.526	19.440	654.362	640.406
BSS 281......	13242	20.527	19.555	650.050	636.474
BSS 282......	13444	20.528	19.865	652.815	652.799
BSS 283......	14982	20.528	19.929	683.080	651.984
BSS 284......	10891	20.529	19.946	637.064	654.441
BSS 285......	10603	20.530	19.548	648.358	636.828
BSS 286......	13577	20.531	19.322	695.771	635.856
BSS 287......	15319	20.531	19.547	677.150	649.156
BSS 288......	13629	20.531	19.670	691.106	643.982
BSS 289......	41514	20.532	19.634	652.845	583.432
BSS 290......	13009	20.532	19.594	714.279	675.590
BSS 291......	14526	20.534	19.719	670.403	632.016
BSS 292......	11902	20.535	19.591	680.951	659.115
BSS 293......	14707	20.536	19.707	671.712	614.140
BSS 294......	10414	20.539	19.564	672.335	614.438
BSS 295......	12438	20.540	19.761	702.380	661.270
BSS 296......	11866	20.541	19.600	645.267	681.357
BSS 297......	13982	20.543	19.706	679.266	685.562
BSS 298......	13417	20.543	19.868	670.957	638.909
BSS 299......	14373	20.545	19.790	668.787	670.565
BSS 300......	12985	20.547	19.862	708.904	678.388
BSS 301......	10150	20.547	19.938	626.381	633.368
BSS 302......	12825	20.548	19.409	686.603	685.971
BSS 303......	13263	20.548	19.605	672.373	625.280
BSS 304......	12134	20.549	19.894	713.490	644.367
BSS 305......	10638	20.550	19.803	693.035	608.847

toward the cluster center than either the HB or RGB stars. (The dashed line shows the combined distribution of the HB + RGB, which are individually quite similar.) Half of the BSS population is within 8″ from the cluster center, compared to only ~20% of the HB or RGB in the same region. The Kolmogorov-Smirnov test applied to the two distributions shows that the probability of drawing the two populations from the same distribution is very small, $\sim 10^{-4}$. This result is consistent with the scenario that BSS are much more massive in population than normal HB and RGB stars. A recent direct spectroscopic mass measured for a BSS in the core of the GGC 47 Tuc (Shara, Saffer, & Livio 1997) also indicates a higher mass for that star.

Extensive *artificial star* tests have been performed to estimate the degree of completeness of the detected BSS population. The completeness level is greater than 80% at the faint edge of the bright sample and ~72% at the faintest magnitude limit. From these results we estimate that the *true* number of BSS in M80 could be as large as ~400.

The number of BSS in M80 is huge. The previous record number was in M3, which has a population of ~170 BSS (about half of the population in M80) in the WFPC2 field of view (Ferraro et al. 1997a). A quantitative comparison requires that the BSS number be normalized to account for the size of the total population. This is done with an appropriate specific frequency:

$$F_{\rm HB}^{\rm BSS} = \frac{N_{\rm BSS}}{N_{\rm HB}} ,$$

where $N_{\rm BSS}$ is the number of BSS and $N_{\rm HB}$ is the number of HB stars in the same area. This ratio can be easily computed in the UV CMDs since the HB population is quite bright and the sequence is well defined. The specific frequency of BSS in M80 turns to be ~1. In other clusters with similar mass, M3, M13, and M92, which have been observed with a similar technique by our group, we find substantially lower values ranging from $F_{\rm HB}^{\rm BSS} \sim 0.17$ for M13 up to 0.55 and 0.67 for M92 and M3. Moreover, considering only the field of view of the PC, the specific frequency of BSS in M80 rises to ~ 1.7, i.e., the BSS are almost twice as abundant as the HB stars.

Several other clusters have recently been surveyed with the WFPC2 covering a region comparable with that of our observations. The somewhat less massive cluster M30 has a population of 48 BSS and a specific frequency $F_{\rm HB}^{\rm BSS} = 0.49$ (Guhathakurta et al. 1998). While not optimal for BSS searches, the survey of Sosin et al. (1997) can give a rough indication of the central BSS population. The clusters with the largest BSS population are NGC 6388 and NGC 2808, each with ~ 100 BSS. These clusters are each about a factor of 4 more massive than M80 but still contain only a fraction (~ 0.3) of the BSS population found in M80. The corresponding specific frequencies of BSS would be about 10% that of M80. Either in terms of number or specific frequency, M80 becomes the Galactic BSS record holder.

4. DISCUSSION

One might speculate that the BSS in M80 are produced by an anomalously large population of primordial binaries. If so, some of these binaries should be detectable outside the cluster core in the form of primordial binary merger BSS, such as those found in the outer region of M3 (Buonanno et al. 1994; Ferraro et al. 1993; Ferraro et al. 1997a). However, recent CMDs of the outer parts of M80 (Brocato et al. 1998; Alcaino et al. 1998) give no indication for a large *primeval* population comparable to that found in M3. Given this, we turn to the structural characteristics of M80 for an explanation.

M80 is much more centrally condensed than M3, M92, and M13, a factor that might promote the production of collisional BSS. Can that factor alone account for the BSS population? We suspect not, because the BSS population in M80 is also large compared with other clusters with high central density. For example, the central part of 47 Tuc is $\log \rho_0 \sim 5.1\ M_\odot\ {\rm pc}^{-3}$ compared to $5.4\ M_\odot\ {\rm pc}^{-3}$ for M80, and is in contrast to $3.5\ M_\odot\ {\rm pc}^{-3}$ for M3 (Pryor & Meylan 1993). Figure 1 of Sosin et al. (1997) shows that 47 Tuc does not have a large population of BSS—no more than 50 BSS can be counted. Likewise, NGC 2808 and NGC 6388 have densities of $\log \rho_0 \sim 4.9$ and $5.7\ M_\odot\ {\rm pc}^{-3}$, respectively, and relatively modest BSS populations.

Since high density cannot account for the large number of BSS in M80, perhaps they arise from its dynamical state. M80 has one of the highest central densities ($\log \rho_0 \sim 5.4\ M_\odot\ {\rm pc}^{-3}$) of any GGC, which has shown no previous evidence for having undergone core collapse (Djorgovski 1993). Generally GGCs are considered core collapsed or not depending on how well their radial distribution of stars is fitted by King models (King 1966). These models are characterized by two parameters, the core radius, r_c, and the tidal radius, r_t, or, alternatively, the concentration, $c = \log(r_t/r_c)$. Our data supplemented with ground-based observations (Brocato et al. 1998) for $r > 85''$ provides the best such test to date for M80.

To determine r_c and c, we first determined the gravity center $C_{\rm grav}$ following the procedure of Montegriffo et al. (1995). We computed $C_{\rm grav}$ by simply averaging the X and Y coordinates (in the local system) of stars lying in the PC camera, and then transforming them to the absolute system. $C_{\rm grav}$ is located at pixel (503 ± 5, 418 ± 5) in our PC image; this corresponds to $\alpha_{\rm J2000} = 16^{\rm h}17^{\rm m}02\overset{\rm s}{.}29$, $\delta_{\rm J2000} = -22°58'32\overset{''}{.}38$, which is $\sim 4''$ northwest of the center reported in the Djorgovski (1993) compilation. The $C_{\rm grav}$ is at pixel (676, 647) in the ground-based coordinate system used in Table 1.

The density profile with respect to the measured gravity center $C_{\rm grav}$ is shown in Figure 4. It was derived using the standard technique (Djorgovski 1988) for all stars with $V < 19.5$. A King model with the most recent values (Trager, Djorgovski, & King 1993), $r_c = 9''$ and $c = 1.95$, does not reproduce the observed density profile for $r < 8''$; however, a King model with a smaller $r_c = 6\overset{''}{.}5$ and essentially the same $c = 2.0$ fits the data reasonably well, as seen in Figure 4.

Meylan & Heggie (1997) warn that it can be difficult to differentiate the dynamical (pre-, in, or postcollapse) phase of a GC on the basis of the shape of the density profile. However, they suggest as a rule of thumb that "*any GC with a concentration* $c \sim 2.0$–2.5 *may be considered as collapsed or on the verge of collapsing or just beyond.*" Thus while the good fit to the King model suggests that M80 has not yet completed core collapse, the value of c is consistent with the suggestion that M80 is on the verge of collapse. The other piece of information we can bring to bear is the anomalously large BSS population. Two post-core collapse clusters have been observed deep enough and with appropriate filters that we have a reasonable estimate of their central BSS populations. Neither of these, 47 Tuc (Sosin et al. 1997) and M30 (Guhathakurta et al. 1998), has a BSS frequency close to that of M80. Thus we see that being in a PCC state cannot explain the BSS population of M80.

The most plausible hypothesis at this point is that the BSS arise from the core collapse process. It is commonly thought that binaries play an important role on the core collapse (Hut et al. 1992; Meylan & Heggie 1997) with the

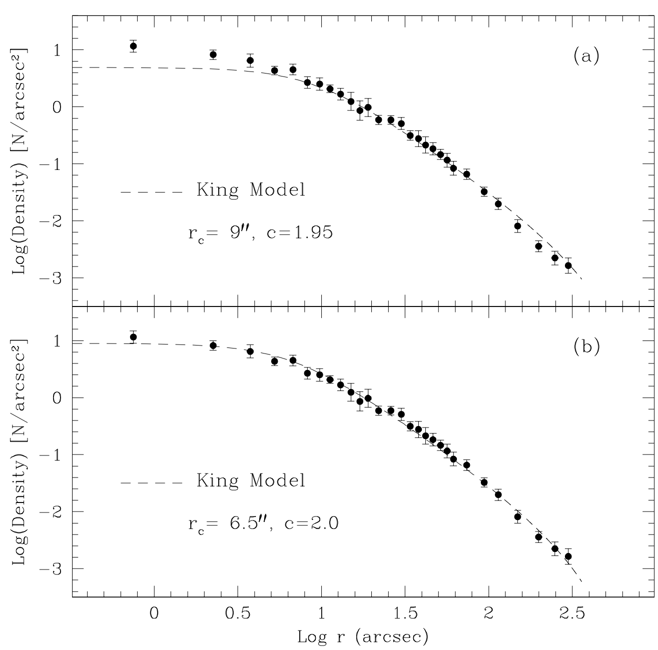

FIG. 4.—Observed radial density profile (*filled circles*) with respect to the center of gravity. The dashed line in (*b*) is the best-fit King model with $r_c = 6\overset{''}{.}5$ and $c = 2.0$.

formation of binaries delaying and eventually halting the collapse. With its high central density, M80 is probably trying very hard to undergo core collapse, but binaries are forming and preventing this from happening. A large population of collision BSS should exist during this time and slightly beyond (until the BSS begin to die off).

This scenario is fully compatible with dynamical evolution times: following Meylan & Heggie (1997), without including binary formation, the entire evolution time (t_{ce}) of the core is $t_{ce} \sim 16t_{rh}(0)$, where $t_{rh}(0)$ is the initial half-mass relaxation time. Using values from Djorgovski (1993), we obtain for M80 $t_{ce} \sim 4 \times 10^8$, which is 30 times smaller than the cluster's age.

5. THE EVOLVED BSS

With such a large population of BSS we might expect to find a significant population of evolved BSS (E-BSS). Renzini & Fusi Pecci (1988) suggested searching for E-BSS during their core helium burning phase since they should appear to be redder and brighter than *normal* HB stars. Following this prescription, Fusi Pecci et al. (1992) identified a few E-BSS candidates in several clusters with predominantly blue HBs where the likelihood of confusing E-BSS stars with true HB or evolved HB stars was minimized. Because of the small numbers, there was always the possibility that some or even most of these candidate E-BSS were due to field contamination. Near cluster centers, field contamination should be less of a problem. In our *HST* study of M3, we identified a sample of E-BSS candidates (see Ferraro et al. 1997b) and argued that the radial distribution of E-BSS was similar to that of the BSS. M80 offers some advantages over M3 in searching for E-BSS: (1) it has a very blue HB, so there should be less confusion between red HB stars and E-BSS; (2) it has a larger number of BSS; and (3) we have identical photometry for M13, which has a very similar blue HB to M80 coupled with a much smaller number of BSS—the E-BSS region of the CMD of M80 should have a substantially larger number of stars than that of M13. In Figure 5 we show a zoomed (U, $U-V$) CMD of the HB region. The expected location for E-BSS has been indicated as a box; 19 E-BSS (*circles*) lie in the box. There are only five E-BSS in the same part of the CMD of M13. V and U magnitudes and position for the E-BSS found in M80 are listed in Table 2.

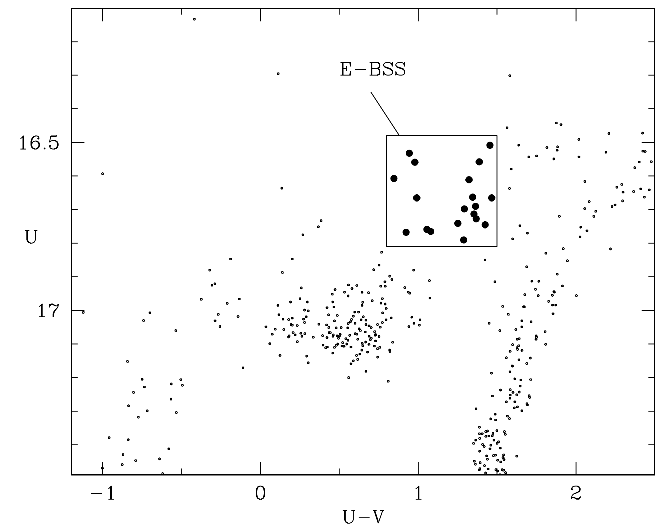

FIG. 5.—Zoomed (U, $U-V$) CMD of the HB region. The E-BSS candidates are plotted as large filled circles.

In the case of M80 it is very unlikely that the E-BSS population is due to background field contamination. In fact, most (15) of the E-BSS have been found in the PC field of view, while only four E-BSS lie in the most external WFs. A estimate of the expected field contamination can be computed adopting the star counts listed by Ratnatunga & Bahcall (1985). Following their model, $\sim$0.6 stars arcmin^{-2} is expected in a section of the CMD, which is *twice* the size of the region used to isolate the E-BSS population. (The E-BSS span less than 1 mag in V, while the Ratnatunga & Bahcall 1985 counts are listed for 2 mag wide bins.) The expected number of field stars is 0 in the PC field of view, and 1.6 stars in the global field of view of the three WF cameras. For this reason we can reasonably conclude that

TABLE 2

THE E-BSS POPULATION IN M80

Name	Identification	V	U	X	Y
E-BSS 1	14764	15.053	16.508	668.291	660.010
E-BSS 2	14945	15.589	16.532	673.819	638.034
E-BSS 3	15346	15.171	16.558	681.072	642.964
E-BSS 4	15350	15.580	16.559	679.837	649.538
E-BSS 5	20898	15.761	16.607	628.347	747.758
E-BSS 6	15300	15.289	16.611	679.280	641.327
E-BSS 7	13422	15.318	16.663	687.622	629.165
E-BSS 8	15333	15.674	16.665	679.198	643.797
E-BSS 9	15273	15.199	16.665	683.524	640.650
E-BSS 10......	13891	15.327	16.690	693.230	665.446
E-BSS 11......	14097	15.406	16.698	670.429	620.216
E-BSS 12......	14710	15.359	16.713	647.164	633.821
E-BSS 13......	30914	15.360	16.727	481.321	614.829
E-BSS 14......	13121	15.490	16.741	656.676	612.601
E-BSS 15......	21514	15.321	16.745	542.077	692.453
E-BSS 16......	13247	15.704	16.759	638.376	645.053
E-BSS 17......	13137	15.686	16.765	633.291	630.344
E-BSS 18......	13220	15.843	16.767	646.076	636.747
E-BSS 19......	43519	15.501	16.790	630.069	622.421

the region of the CMD used to select an E-BSS candidate is essentially unaffected by field contamination.

The cumulative radial distribution of the E-BSS stars is shown in Figure 3 (*dotted line*). The E-BSS cumulative distribution is quite similar to the BSS distribution and significantly different from that of the HB-RGB. A Kolmogorov-Smirnov test shows that the probability that the E-BSS and BSS population has been extracted from the same distribution is $\sim$67%, while the probability that the E-BSS and the RGB-HB population have the same distribution is only $\sim$1.6%. This result confirms the expectation that the E-BSS share the same distribution of the BSS, and they are both a more massive population than the bulk of the cluster stars. It further strengthens the case that field contamination is negligible.

Earlier studies (Fusi Pecci et al. 1992; Ferraro et al. 1997a) have suggested that the ratio of bright BSS (b-BSS) to E-BSS is $N_{\text{b-BSS}}/N_{\text{E-BSS}} \approx 6.5$. For M80 the number of b-BSS (defined as in Ferraro et al. 1997a) is $N_{\text{b-BSS}} = 129$, and we find $N_{\text{b-BSS}}/N_{\text{E-BSS}} = 6.8$ fully consistent with earlier studies. Because both our BSS and E-BSS samples are so cleanly defined, the ratio of the total number of BSS to E-BSS, $N_{\text{BSS}}/N_{\text{E-BSS}} \sim 16$, should be useful in testing lifetimes of BSS models.

6. CONCLUSIONS

The emerging scenario for BSS is complex. All GGCs that have been properly surveyed have some BSS, so BSS must be considered as a normal component of GGC population. BSS are found in diverse environments and are probably formed by both merging primordial binaries and stellar collisions. Some intermediate low-density clusters have only a few BSS (M13), while similar clusters (M3 and M92) have many more. This may arise from the fact that the initial population of binaries in clusters like M13 is small. The relatively large population of BSS in the exterior of M3 (Ferraro et al. 1997a) in contrast to the absence of BSS in the exterior of M13 (Paltrinieri et al. 1998) supports the notion of very different primordial binary populations.

The densest cluster cores have significant but highly variable BSS populations (see the discussion in Ferraro et al. 1995). In particular, the post–core-collapse clusters 47 Tuc and M30 have significantly smaller BSS populations than M80.

We suggest that the exceptional population in M80 arises because we have caught a cluster at a critical phase in its dynamical evolution. This effect could be enhanced by a large fraction of primordial binaries, but there is no indication for this in the form of a large BSS population in the outer cluster (Brocato et al. 1998; Alcaino et al. 1998). More information is needed before a definitive conclusion can be reached. A search for other indications of a high frequency of stellar multiplicity in M80, such as a broadening of the main sequence, would also be very useful. Also, further study of the velocity distribution would be important to clarify the dynamical state of the cluster (Meylan & Heggie 1997). Core collapse is one of the most spectacular phenomena in nature. It is important to confirm whether we have caught M80 during the period when the stellar interactions are delaying the collapse of the core (and producing BSS).

This research was partially financed by the Agenzia Spaziale Italiana (ASI). F. R. F. acknowledges MURST financial support for the project Stellar Evolution and the ESO Visitor Program for its hospitality. R. T. R. and B. D. are supported in part by the NASA Long-Term Space Astrophysics grant NAG 5-6403 and STScI/NASA grants GO-6607 and GO-6804.

REFERENCES

Alcaino, G., Liller, W., Alvarado, F., Kravtsov, V., Ipatov, A., Samus, N., & Smirnov, O. 1998, AJ, 116, 2415
Bailyn, C. D. 1995, ARA&A, 33, 133
Brocato, E., Castellani, V., Scotti, G. A., Saviane, I., Piotto, G., & Ferraro, F. R. 1998, A&A, 335, 929
Buonanno, R., Corsi, C. E., Buzzoni, A., Cacciari, C., Ferraro, F. R., & Fusi Pecci, F. 1994, A&A, 290, 69
Djorgovski, S. G. 1988, in The Harlow-Shapley Symp. on Globular Cluster Systems in Galaxies, ed. J. E. Grindlay & A. G. D. Philip (Dordrecht: Kluwer), 333
———. 1993, in ASP Conf. Ser. 50, Structure and Dynamics of Globular Clusters, ed. S. G. Djorgovski & G. Meylan (San Francisco: ASP), 373
Drissen, L., & Shara, M. M. 1998, AJ, 115, 725
Ferraro, F. R., et al. 1997a, A&A, 324, 915
Ferraro, F. R., Fusi Pecci, F., & Bellazzini, M. 1995, A&A, 294, 80
Ferraro, F. R., Fusi Pecci, F., Cacciari, C., Corsi, C., Buonanno, R., Fahlman, G. G., & Richer, H. B. 1993, AJ, 106, 2324
Ferraro, F. R., Paltrinieri, B., Fusi Pecci, F., Cacciari, C., Dorman, B., & Rood, R. T. 1997b, ApJ, 484, L145
Ferraro, F. R., & Paresce, F. 1993, AJ, 106, 154
Fusi Pecci, F., Ferraro, F. R., Corsi, C. E., Cacciari, C., & Buonanno, R. 1992, AJ, 104, 1831
Guhathakurta, P., Webster, Z. T., Yanney, B., Schneider, D. P., & Bahcall, J. N. 1998, AJ, 116, 1757
Hills, J. G., & Day, C. A. 1976, Astrophys. Lett., 17, 87
Hut, P., et al. 1992, PASP, 104, 981
King, I. R. 1966, AJ, 71, 64
Meylan, G., & Heggie, D. G. 1997, A&A Rev., 8, 1
Montegriffo, P., Ferraro, F. R., Fusi Pecci, F., & Origlia, L. 1995, MNRAS, 276, 739
Paltrinieri, B., Ferraro, F. R., Fusi Pecci, F., & Carretta, E. 1998, MNRAS, 293, 434
Paresce, F., Shara, M., Meylan, G., Baxter, D., & Greenfield, P. 1991, Nature, 352, 297
Pryor, C., & Meylan, G. 1993, in ASP Conf. Ser. 50, Structure and Dynamics of Globular Clusters, ed. S. G. Djorgovski & G. Meylan (San Francisco: ASP), 357
Ratnatunga, K. U., & Bahcall, J. N. 1985, ApJS, 59, 63
Renzini, A., & Fusi Pecci, F. 1988, ARA&A, 26, 199
Sandage, A. R. 1953, AJ, 58, 61
Shara, M. M., Saffer, R. A., & Livio, M. 1997, ApJ, 489, L59
Sosin, C., Piotto, G., Djorgovski, S. G., King, I. R., Rich, R. M., Dorman, B., Liebert, J., & Renzini, A. 1997, in Advances in Stellar Evolution, ed. R. T. Rood & A. Renzini (Cambridge: Cambridge Univ. Press), 92
Trager, S. C., Djorgovski, S. G., & King, I. R. 1993, in ASP Conf. Ser. 50, Structure and Dynamics of Globular Clusters, ed. S. G. Djorgovski & G. Meylan (San Francisco: ASP), 347